Journal of Building Engineering 44 (2021) 102717

Contents lists available at ScienceDirect

Journal of Building Engineering

journal homepage: www.elsevier.com/locate/jobe

Enhancing self-stress sensing ability of smart ultra-high performance concretes under compression by using nano functional fillers

Huy Viet Le [a,b], Min Kyoung Kim [a], Seon Uk Kim [a], Sang-Yeop Chung [a], Dong Joo Kim [a,*]

[a] Department of Civil and Environmental Engineering, Sejong University, 209, Neungdong-ro, Gwangjin-gu, Seoul, 143-747, South Korea
[b] Department of Civil Engineering, Hanoi University of Mining and Geology, Hanoi, Viet Nam

ARTICLE INFO

Keywords:
Smart ultra-high-performance concrete (S-UHPC)
Self-sensing
Steel slag aggregate
Nickel aggregate
Copper aggregate
MWCNT

ABSTRACT

Smart ultra-high performance concretes (S–UHPCs) with high self-stress sensing abilities have great application potential for monitoring the loss of prestressing stress in steel tendons to predict structural failure. This study aimed to enhance the self-stress sensing ability of compressed S–UHPCs by employing different types of electrically conductive functional fillers, including fiber type (short smooth steel fibers), particle type (fine steel slag aggregates, FSSAs; nickel aggregates, NAs; and copper aggregates, CPAs), and nano type (multiwall carbon nanotubes, MWCNTs). The S–UHPCs containing CPAs exhibited the highest electrical conductivity due to the high electrical conductivity of the CPAs. However, the S–UHPCs containing a combination of steel fibers, FSSAs, and MWCNTs produced the highest fractional change in electrical resistivity (56.8%) and stress sensitivity coefficient (0.41%/MPa).

1. Introduction

Smart construction materials (SCMs) have demonstrated their self-sensing ability much expected to be applicable to structural health monitoring systems to predict and prevent the sudden failure of structures. Specifically, the potential of these SCMs has been demonstrated for monitoring the loss of prestressing stress in prestressing steel tendons [1]. The self-sensing ability of SCMs is based on a change in electrical resistance (or resistivity) corresponding to the change in the electrically conductive networks within the SCM under load [2–11]. The conductive networks may operate via three different mechanisms, namely (1) ionic conduction in a continuous pore solution system, (2) tunneling conduction, and (3) contact conduction between electrically conductive functional fillers [2]. The addition of electrically conductive functional fillers is generally preferred to construct the conductive network within an SCM and be able to enhance the self-sensing capacities of the SCMs. Commercial functional fillers commonly used in SCMs include carbon fibers (CFs) [3,10,12–19], carbon nanofibers (CNFs) [20], carbon black (CB) [17,21–23], carbon nanotubes (CNTs) [3,10,24–30], multi-wall CNTs (MWCNTs) [31–35], graphite nanofibers (GNFs) [27,36], graphene [27], nickel [37], and steel fibers [38–41]. Chung [13] reported that the cement-based materials containing discontinuous fibers have effective sensing capacity to sense their own strain. Moreover, piezoresistive cement-based sensor containing carbon fiber (6 mm length) can be used to achieve as sensitivity of 1.35%/MPa when the stress was in the range from 0 MPa to 8 MPa [17].

The self-stress sensing capacity of SCMs is mostly valid until 20 MPa compressive stress because of the limited compressive strength of SCM matrices [42]. The formation of cracks within SCMs under the compressive stress caused a nonlinear correlation between the electrical resistivity response of SCMs and applied stress [42]. Further, achieving uniform distribution of the functional fillers in high strength mortars and/or concretes remains a challenge, especially in ultra-high-performance concrete (UHPC). You et al. [43] reported that a minimal change in the electrical resistivity of a compressed smart UHPC containing steel fibers and MWCNTs, when the compressive stress was in the elastic region, was owing to poor distribution of the MWCNTs in the UHPC matrix. A smart ultra-high performance concretes (S-UHPC) with steel fibers and fine steel slag aggregates (FSSAs) instead of silica sand has been recently developed [42,44]. The FSSAs in the S-UHPC were spherical with a maximum diameter of 0.39 mm, and could be more uniformly distributed within the UHPC matrix [42,44]. The fractional

Abbreviations: AC, alternative current; NA, nickel aggregate; CPA, copper aggregate; DC, direct current; FCR, fractional change in electrical resistivity; FSSA, fine steel slag aggregate; MWCNT, multiwall carbon nanotube; PS, prestressing steel; SCM, smart construction material; SSC, stress sensitive coefficient; S-UHPC, smart ultra-high-performance concrete; UHPC, ultra-high-performance concrete.

* Corresponding author.
E-mail address: djkim75@sejong.ac.kr (D.J. Kim).

https://doi.org/10.1016/j.jobe.2021.102717
Received 23 March 2021; Received in revised form 7 May 2021; Accepted 10 May 2021
Available online 14 May 2021

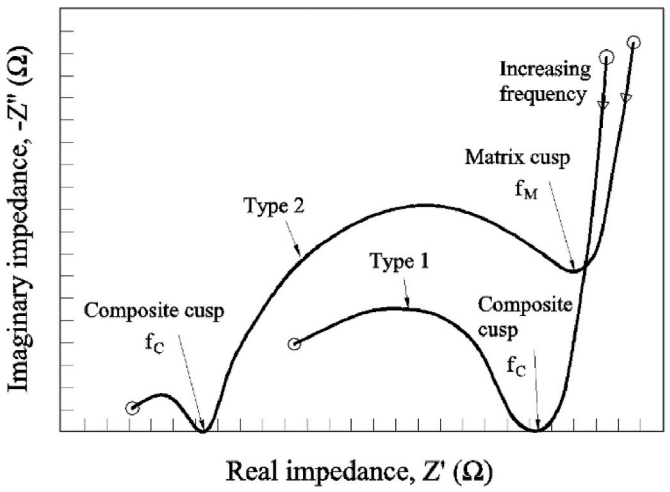

Fig. 1. Typical AC impedance response of the SCMs.

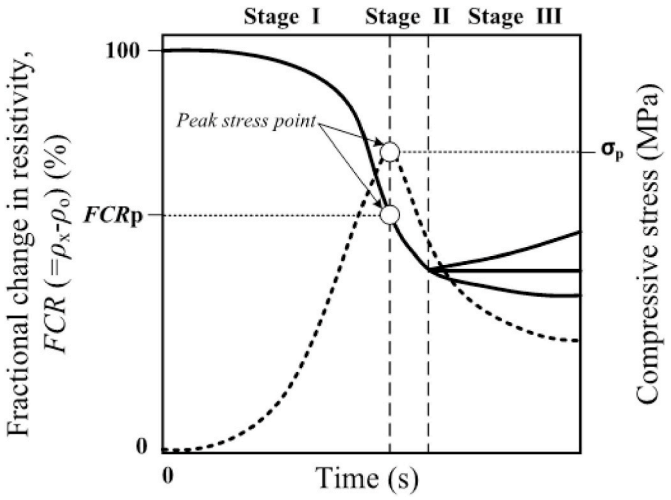

Fig. 2. Typical piezoresistive response of S–UHPCs under compression.

change in electrical resistivity (*FCR*) of the S–UHPCs containing steel fibers (2 vol%) and FSSAs (0.5 wt% of cement) was 42.9% at the peak compressive stress (144 MPa) [44].

This study aimed to further improve the self-stress sensing ability of S–UHPCs by improving the conductive network and electrical conductivity of functional fillers. Various electrically conductive functional fillers, nickel aggregates (NAs), copper aggregates (CPAs), FSSAs, steel fibers, and MWCNTs, were investigated to increase the tunneling conduction and/or contact conduction in the conductive network within matrix under compressive stress. The particle functional fillers (i.e. NAs, CPAs, and FSSAs) were used to partially replace silica sands in the SCM matrices to enhance the electrical conductivity via quantum tunneling effects. Short smooth steel fibers were included in the S–UHPCs to improve the electrically conductive network as well as to prevent micro cracks within the linear elastic region. The MWCNTs (nano type functional filler) were also added to improve the electrically conductive network on the nano-level via tunneling effects. The specific objectives of the study are to (1) compare the effect of various types and contents of electrically conductive particle type functional fillers on the electrical resistivity and piezoresistive response of S–UHPCs under compression, and (2) investigate the effect of adding nano type functional filler to the UHPC matrix on the piezoresistive response of the S–UHPCs.

2. AC impedance spectroscopy and typical electrical resistivity response of S–UHPCs under compression

Alternating current (AC) measurements are generally preferred over direct current (DC) measurements for the enhancement of the electrical properties of cement composites to avoid electrical polarization over time due to ion migration [45,46]. Thus, the two probe AC measurement method was used in this study.

The typical AC impedance spectroscopy results of the SCMs are presented as Nyquist plots, where the imaginary impedance ($-Z''$) was plotted against the real impedance (Z') (Fig. 1) [47–50]. The plots were parameterized in terms of frequency, which decreased from left (high frequency) to right (low frequency) [50]. The Nyquist plot of a cementitious composite with a single arc (Type 1) gives the electrical resistance (R_C) and imaginary impedance ($-Z''_C$ for capacitance) of the cementitious composite at the cusp of the plot. The resistance and imaginary impedance of cementitious composite with two arcs (Type 2) are determined based on the real and imaginary impedance at the cusp on the left side (high frequency) between the two material arcs, which is referred to as the composite cusp. The electrical resistivity (ρ) of the composite was calculated from the measured composite resistance (R) as follows:

$$\rho = R\frac{A}{L} \tag{1}$$

where A is the cross-sectional area, and L is the gauge length between the two electrodes.

Fig. 2 illustrated the typical piezoresistive response of S–UHPCs containing different functional fillers in three stages [42,44,51]. Firstly, the electrical resistivity decreased rapidly as the compressive stress increased from 0 to the peak stress (σ_p) (Stage I), after which it decreased continuously to a minimum electrical resistivity as the compressive stress decreased (Stage II), finally stabilizing, slightly increasing and/or decreasing as the compressive stress continued to decrease (Stage III).

In the elastic stage, the reduction in electrical resistivity of S–UHPCs was dependent on both contacting and tunneling conduction between the functional fillers [42,44,51]. As the compressive stress increased, the compressive strain increased, the distance between functional fillers was closer, the number of contacting between functional fillers increased, and consequently the contacting and tunneling conductions as well as the total conductivity of S–UHPCs increased, i.e., the electrical resistivity of S–UHPCs decreased. After matrix cracking, the piezoresistive response of the S–UHPCs would be mainly dependent on contacting conduction. As the compressive stress increased, the number of contacting steel fibers increased at the cracked positions. The contact between the steel fibers at the cracked positions significantly decreased the electrical resistivity [44]. At the peak stress of S–UHPCs under compression, contacting conduction between steel fibers at the cracked parts would be the main factor influencing the reduction in electrical resistivity of the S-UHPC composites. After peak stress, the number of contacting steel fibers at cracked parts continuously increased with increasing compressive stress. Thus, the electrical resistivity of S–UHPCs decreased continuously to a minimum value at a stable stage of the conductive network. Then, a slight increase in electrical resistivity as compressive strain continuously increased would be attributed to the widening of micro-cracks.

The tunneling conduction was depended on the distance between functional fillers, the electrical conductivity of functional fillers, and the electrical conductivity of matrix while the contacting conduction was mainly depended on the content and type of functional fillers [2,42,44,52,53]. Thus, in this study, to improve tunneling and contacting conduction of S–UHPCs, the different high electrical conductivity materials (nickel, copper, and steel slag aggregates) was used as functional fillers. In addition, nano conductive materials (MWCNTs) was used to combine with different types of functional fillers including fiber type (steel fibers) and a particle type functional fillers to improve both tunneling and contacting conductions of S–UHPCs.

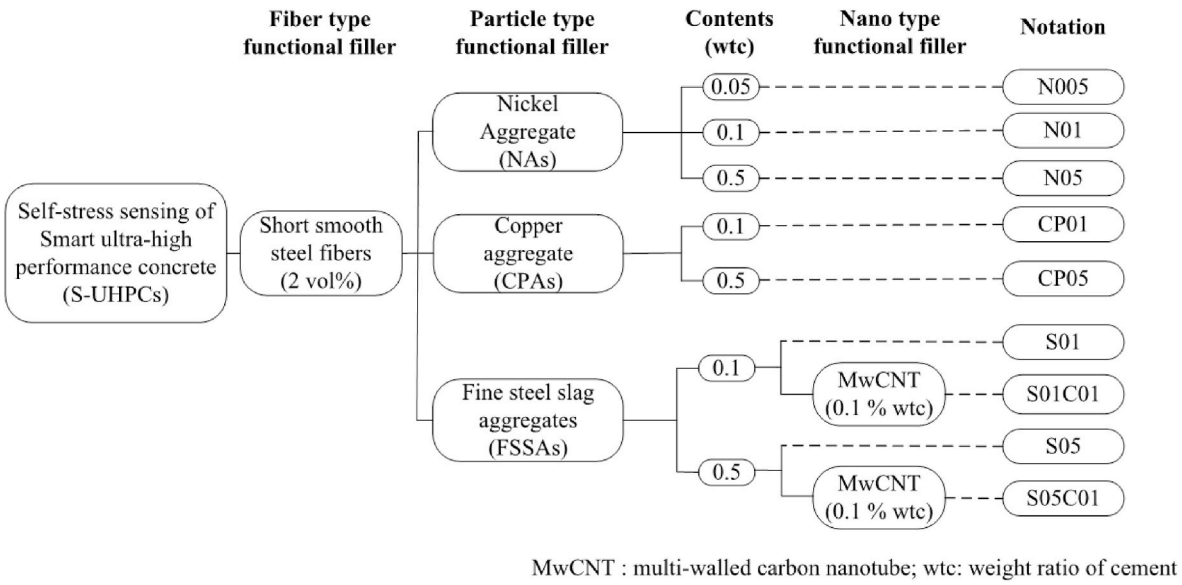

Fig. 3. Experimental design for enhancing the self-stress sensing ability of S–UHPCs.

Table 1
Properties of the functional fillers.

Functional filler	Size (mm)	Length (mm)	Density (g/cm^3)	Elastic modulus (GPa)	Electrical conductivity (10^6 Sm^1) ([a])	Cost (Krw/kg)
Steel fiber	0.2	6	7.85	200	11.2	12000
FSSA	<0.39	–	3.56	–	11.2	190
NA	0.01	–	6.90	210	16.4	88000
CPA	0.14	–	6.96	110	64.1	67000
MWCNT	10.10^{-6}	0.01	0.02–0.04	–	0.2	3000000

[a] Referred from Ref. [55]. The electrical conductivity values of steel fiber and FSSA are assumed to equal those of iron. Krw: Korean won.

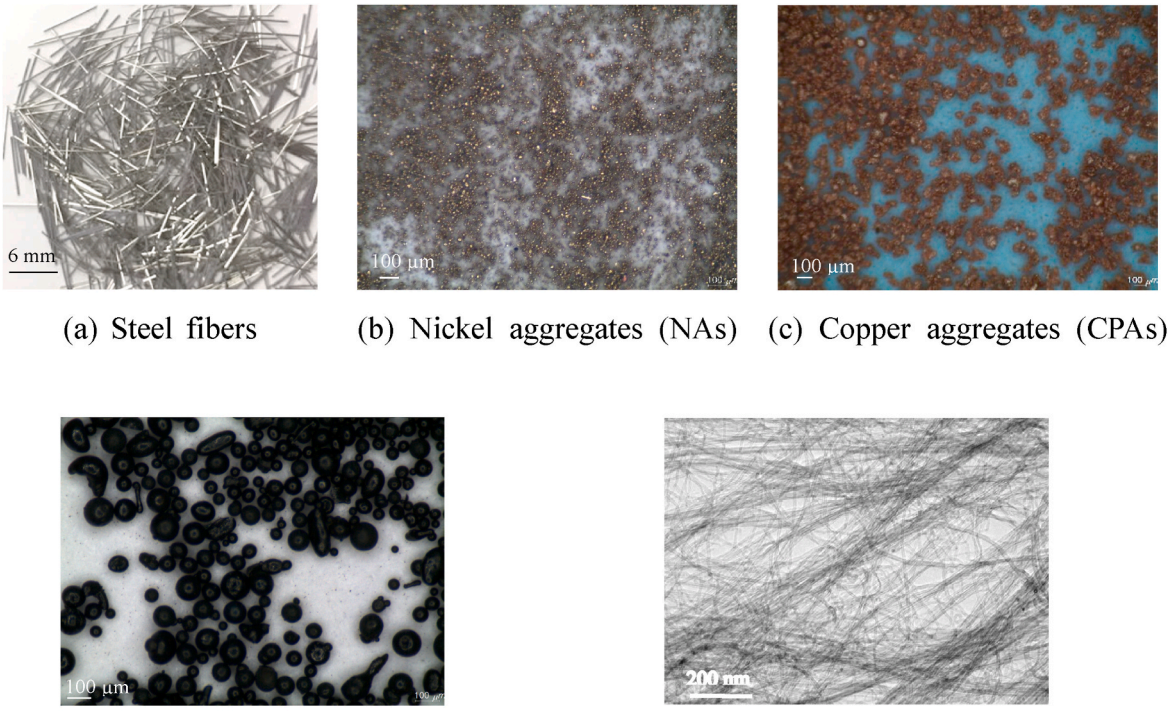

(a) Steel fibers (b) Nickel aggregates (NAs) (c) Copper aggregates (CPAs)

(d) Fine steel slag aggregates (FSSAs) (e) Multi-wall carbon nanotubes (MWCNTs)

Fig. 4. Images of the functional fillers.

Table 2
Composition (weight ratio), flow, compressive strength, and density of the S–UHPCs.

Test series	C	SF	SP	SS	NA	CPA	FSSA	MWCNT	W	SPP	Steel fiber (vol %)	Flow (mm)	fc (MPa)	γ (kg/m^3)
N005	1	0.15	0.25	0.95	0.05	–	–	–	0.2	0.087	2	250	156.1	2460
N01	1	0.15	0.25	0.9	0.1	–	–	–	0.2	0.085	2	230	167.8	2498
N05	1	0.15	0.25	0.5	0.5	–	–	–	0.2	0.094	2	250	156.0	2747
CP01	1	0.15	0.25	0.9	–	0.1	–	–	0.2	0.085	2	250	158.2	2474
CP05	1	0.15	0.25	0.5	–	0.5	–	–	0.2	0.1	2	240	165.0	2712
S01	1	0.15	0.25	0.9	–	–	0.1	–	0.2	0.071	2	230	155.9	2464
S05	1	0.15	0.25	0.9	–	–	0.5	–	0.2	0.071	2	275	179	2554
S01C01	1	0.15	0.25	0.9	–	–	0.1	0.001	0.2	0.096	2	200	159.1	2423
S05C01	1	0.15	0.25	0.5	–	–	0.5	0.001	0.2	0.096	2	200	160.1	2573

C: cement; SF: silica fume; SP: silica powder; SS: silica sand; NA: nickel aggregate; CPA: copper aggregate; FSSA: fine steel slag aggregate; MWCNT: multiwall carbon nanotube; W: water; SPP: superplasticizer; fc: compressive strength; γ: density.

Besides, it should be noted that the content and electrical conductivity of functional fillers should be controlled to maximize the piezoresistivity of smart concretes according to percolation threshold theory: as the initial conductivity of smart concrete was over percolation threshold, the piezoresistivity response of smart concretes decreased [44,54]. Hence, effect of different functional filler contents was also investigated in this study to find a maximum the self-stress sensing ability of S–UHPCs.

3. Experimental methodology

Fig. 3 illustrates an experimental program designed to investigate the self-stress sensing abilities of S–UHPCs corresponding to different functional fillers. Nine series of test specimens were prepared as shown in Fig. 3.

3.1. Materials and specimen preparation

Table 1 provides the properties of the functional fillers, including size, length, density, elastic modulus, electrical conductivity, and cost while Fig. 4 shows the images of the steel fibers, nickel aggregates (NAs), copper aggregates (CPAs) and fine steel slag aggregates (FSSAs) captured by using a stereoscopic microscope equipped with a Lusis digital camera HC-30MU (Huvitz, Republic of Korea) and the field emission scanning electron microscope (FE-SEM) image of the multi-walled carbon nanotubes (MWCNTs). The length and diameter of short smooth steel fibers, used in this study as a fiber type functional filler, was 6 and 0.2 mm. The NAs (average diameter, 0.01 mm), CPAs (average diameter, 0.14 mm), and spherical FSSAs (maximum diameter, 0.39 mm) were used to investigate the effects of particle type functional fillers on the electrical and piezoresistive response of S–UHPCs. The FSSAs comprised electric arc furnace (EAF) steel slag produced by Ecomaister Co. Ltd. via slag atomizing technology (SAT). Moreover, MWCNTs (0.01 mm length and 10 nm diameter) were added to the S–UHPCs containing steel fibers and FSSAs to investigate the effect of nano type functional filler. The purity of the MWCNTs was more than 99 wt% with a specific surface area of 150–200 m^2/g. The electrical conductivity of functional fillers was referred from Ref. [55].

Table 2 provides the composition of the S–UHPCs corresponding to different functional fillers. Cement Type I (ASTM standard) and silica sand (average diameter, 0.2 mm) were used, as well as a polycarboxylate-based superplasticizer containing 30% solids and 70% water. 2 vol% of steel fibers were added to all specimens, while silica sand in the S-UHPC was partially replaced with one of three particle type functional fillers, namely NAs, CPAs, either FSSAs. The ratio of functional fillers to cement (by weight) was either 0.05, 0.1 or 0.5 for the NAs, and either 0.1 or 0.5 for the CPAs and FSSAs to investigate the effect of functional filler content on the self-stress sensing of the S–UHPCs.

The terms N, CP, S, and C were used to assign sample codes to S-UHPC matrices containing NAs, CPAs, FSSAs, and MWCNTs, respectively. Further, functional filler to cement ratios of 0.05, 0.1, or 0.5 was coded as 005, 01, or 05, respectively. Thus, nine S-UHPC matrices were evaluated with sample codes N005, N01, N05, CP01, CP05, S01, S05, S01C01, and S05C01. Test results of S05 was adopt from Ref. [44].

The S-UHPC specimens without MWCNTs (N005, N01, N05, CP01, CP05, and S01) were prepared by dry-mixing cement, silica fume, silica powder, silica sand, and the particle type functional fillers (NAs, CPAs or FSSAs) for 3 min in a 20*l* Hobart-type laboratory mixer. Water was slowly added and mixing was continued for another 3 min. A superplasticizer was gradually added and mixing was continued for another 5 min. Flow testing of the mixture was conducted, where a flow value of

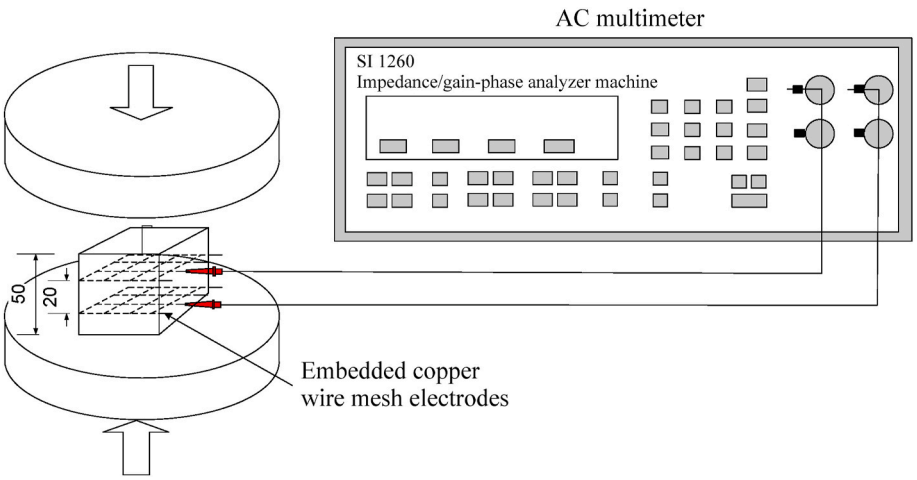

Fig. 5. Experimental set-up for AC impedance spectroscopy.

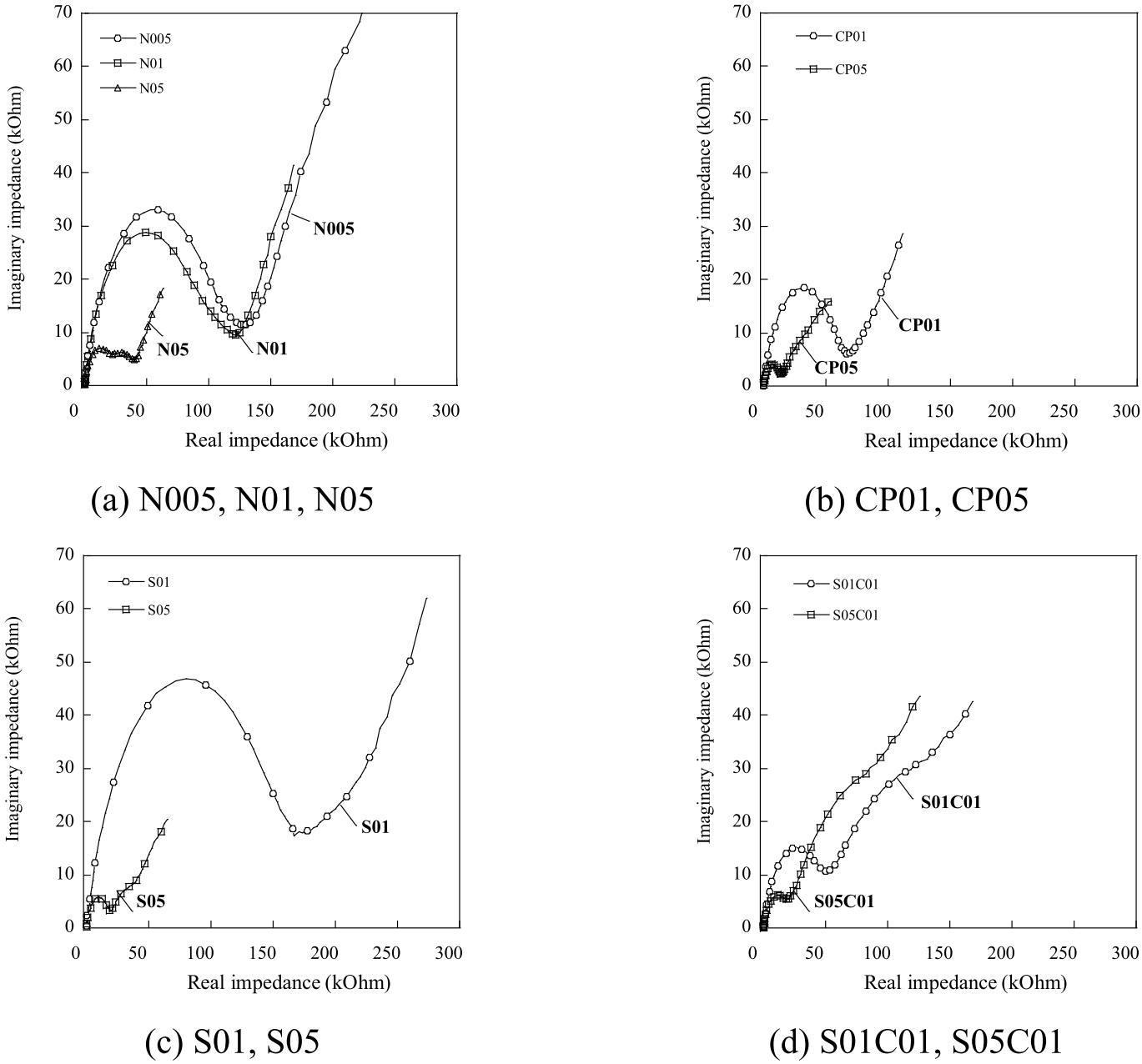

Fig. 6. AC impedance response of S–UHPCs corresponding to the different particle type functional fillers.

220 and 250 mm indicated that a suitable workability was achieved for uniform fiber distribution (Table 2). The steel fibers were dispersed manually into the mixture, followed by machine mixing for a further 1 min.

The S-UHPC specimens containing 1.0% MWCNTs (S01C01 and S05C01), as nano type functional filler, were prepared by initially distributing the MWCNTs in water using a sonicator with a sonification amplitude of 50% for 2 h. The water containing MWCNTs was pre-mixed with half of the superplasticizer. Cement, silica sand, silica powder, and silica fume were dry-mixed separately for 5 min. The water containing MWCNTs and superplasticizer was gradually added to the dry mixture and mixing was continued for 3 min. The remaining half of the superplasticizer was added and mixing was continued until the mixture exhibited suitable workability. Then, the short smooth steel fibers were added and mixing was continued for 1 min.

The S-UHPC mixtures were poured into cubic molds (50 × 50 × 50 mm^3) and a slight vibration was applied. During the casting, copper-wire mesh (height = 70 mm; width = 45 mm) was embedded into the specimens as electrodes with 20 mm distance between electrodes. The specimens for compressive strength measurement were additionally manufactured without adding electrodes. All the specimens were covered with a plastic sheet and stored in the laboratory at 20 ± 2 °C for 48 h before demolding. After demolding the specimen, the specimens were cured in a hot water (90 °C) for three days and kept in the laboratory at 20 ± 2 °C for 5 days prior to testing.

3.2. Test methods and procedures

AC impedance spectroscopy and the piezoresistive response of the S-UHPC specimens were measured by using a SI 1260 impedance/gain-phase analyzer via the two-probe method (Fig. 5). The two-probe method was applied for the electrical impedance measurement because the dimension of cubic specimen (50 × 50 × 50 mm^3) was not large enough to include four electrodes for applying the four-probe

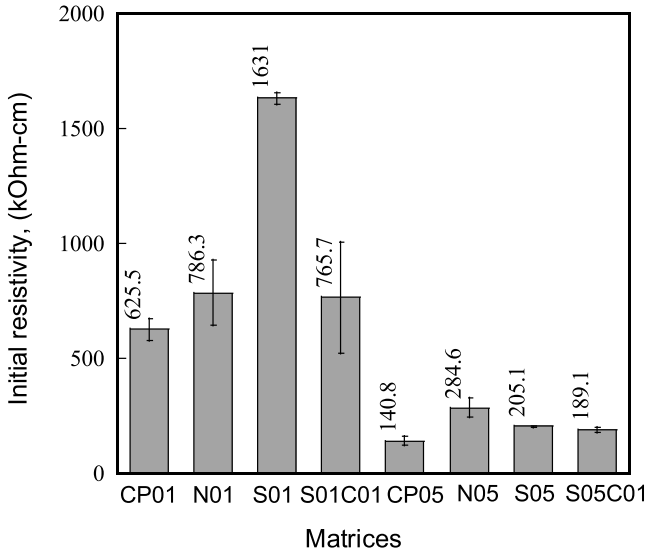

Fig. 7. Effect of different functional fillers on the initial electrical resistivity of S–UHPCs.

method. Moreover, two-probe method also could successfully measure the change in electrical resistance under load, although it obtained higher electrical resistance due to the contact resistance between electrode and specimen [26,27]. The frequency of the AC multimeter varied between 0.1 Hz and 10 MHz at a constant voltage of 250 mV to obtain the AC impedance spectra prior to measuring the change of electrical impedance of the S-UHPC under compression. The piezoresistive response of the S–UHPCs was measured under compression at the fixed frequency determined at the composite cusp point in the AC impedance spectroscopy results of the S-UHPC matrix. A universal testing machine (UTM) was used to apply a compressive load to the specimens by maintaining a displacement speed of 1 mm/min during loading. The cubic specimens per test series without embedded copper-wire mesh were tested to obtain the average compressive strength of S–UHPCs.

FE-SEM images and energy-dispersive X-ray spectroscopy (EDS) analysis were obtained by using a Hitachi SU8010 instrument at Sejong University (Seoul, South Korea). SEM images at the interfacial transition zone (ITZ) between functional fillers and matrix were captured to show micro structures of matrices surrounding functional fillers while EDS images of Cu, Fe, Ni, and C (carbon) elements in matrices were captured to examine the distribution of copper, steel slag, nickel aggregates, and MWCNTs in matrices, respectively. The Hitachi SU8010 instrument with the applied accelerating voltage of 30 kV is capable of obtaining high contrast EDS images of light element materials such as C element [56]. The applied accelerating voltage was 15 kV for capturing EDS images of Cu, Fe, and Ni elements while that was 30 kV for capturing EDS images of C element. The SEM-EDS specimens were prepared from S-UHPC matrix according to three steps including cutting, grinding and polishing, and roughness checking [57].

4. Results

4.1. Effect of different particle type functional fillers on the electrical response of S–UHPCs

Fig. 6 shows the effects of different particle type functional filler and the amount of those on the measured AC impedance spectroscopy of the S–UHPCs. The Nyquist plot of cement mortar presented a cusp point like Type 1 in Fig. 1 whereas those of S05, N05, S05C01, and S01C01 matrices did two cusp points like Type 2 in Fig. 1.

Fig. 7 compares the initial electrical resistivity of S–UHPCs containing different particle type functional fillers. The initial electrical resistivity of the S–UHPCs was calculated using Eq. (1) based on the real impedance at the composite cusp point for Type 1 and at the left cusp point for Type 2 in Fig. 1. The initial electrical resistivity of S05 has been previously investigated [44], which revealed that the addition of functional fillers with high electrical conductivity enhanced the electrically conductive pathways in the composite. As can be seen in Fig. 7, the S–UHPCs containing CPAs (CP series) exhibited lower electrical resistivity than those containing NAs (N series) or FSSAs (S series). Specifically, CP05 exhibited the lowest electrical resistivity of 140.8 kΩ-cm.

4.2. Effect of different functional fillers on the electromechanical response of S–UHPCs under compression

Fig. 8 shows the piezoresistive response of S–UHPCs containing different functional fillers including particle and nano type: Fig. 8a–c, d-e, f-g, and h-i shows that containing NAs, CPAs, FSSAs, and MWCNTs, respectively. As can be seen in Fig. 8, the piezoresistive response of all S–UHPCs can be divided into three main stages like typical piezoresistive response in Fig. 2. An increase in compressive stress or strain generally led to a decrease in electrical resistivity of the S–UHPCs. The fractional change in electrical resistivity (*FCR*) and stress sensitive coefficient (*SSC*) of S–UHPCs can be calculated according to Eq. (2) and Eq. (3), respectively.

$$FCR = \frac{|\Delta\rho|}{\rho_0} \times 100 = \frac{|\rho_p - \rho_0|}{\rho_0} \times 100\ [\%] \tag{2}$$

$$SSC = \frac{FCR}{\sigma_p}\ [\%\text{MPa}] \tag{3}$$

where ρ_p is the electrical resistivity of the S–UHPCs at peak stress, ρ_0 is the initial electrical resistivity of the S–UHPCs, and σ_p is peak stress of the S–UHPCs. Table 3 summarized the self-stress sensing characteristics (ρ_0, $\Delta\rho$, *FCR*, σ_p, and *SSC*) of the S–UHPCs corresponding to the different functional fillers.

The addition of FSSAs generally produced higher *FCR* of S–UHPCs than that of CPAs and NAs, regardless content of FFs, as shown in Fig. 9. S05 exhibited the highest *FCR* (42.9%) and *SSC* (0.298%/MPa) among the investigated test series of S–UHPCs containing particle FFs. Besides, the higher content of FSSAs from 0.1 to 0.5 clearly produced the higher *FCR* from 26.5 to 42.9%, whereas the addition of FSSAs more than cement, i.e., the weight ratio of FSSAs per cement was more than 1.0, considerably decreased the *FCR* from 42.9 to 34.4% [44]. The higher content (weight per cement) of CPAs from 0.1 to 0.5 produced a slight reduction in the *FCR* of the S–UHPCs from 17.1 to 15.8%. And, the higher content of NAs from 0.05 to 0.5 generated a noticeable reduction in *FCR* from 27.5 to 15.6%.

The addition of MWCNTs clearly improved both the electrical conductivity and piezoresistive response of S–UHPCs. The initial resistivity of F2S05C01 and F2S01C01 was 189.1 and 765.7 kΩ-cm, respectively, which was clearly lower than that of the S–UHPCs without MWCNTs, where F2S05 and F2S01 were 205.1 and 1631.4 kΩ-cm, respectively, as provided in Table 4. Fig. 9 compares the FCR and SSC of the S–UHPCs with and without MWCNTs and reveals that the addition of MWCNTs increased the FCR regardless of the FSSA content. F2S05C01 exhibited the highest *FCR* (56.8%) and *SSC* (0.41%/MPa) among all of the S-UHPC samples (Table 4), thereby demonstrating that the combination of FF_f (steel fibers), FF_p (FSSAs), and FF_n (MWCNTs) produced a good conductive network.

4.3. Physical properties and microstructure of S–UHPCs corresponding to the different functional fillers

As provided in Table 2, the addition of functional fillers including NAs, CPAs, FSSAs, and MWCNTs generally increased the compressive

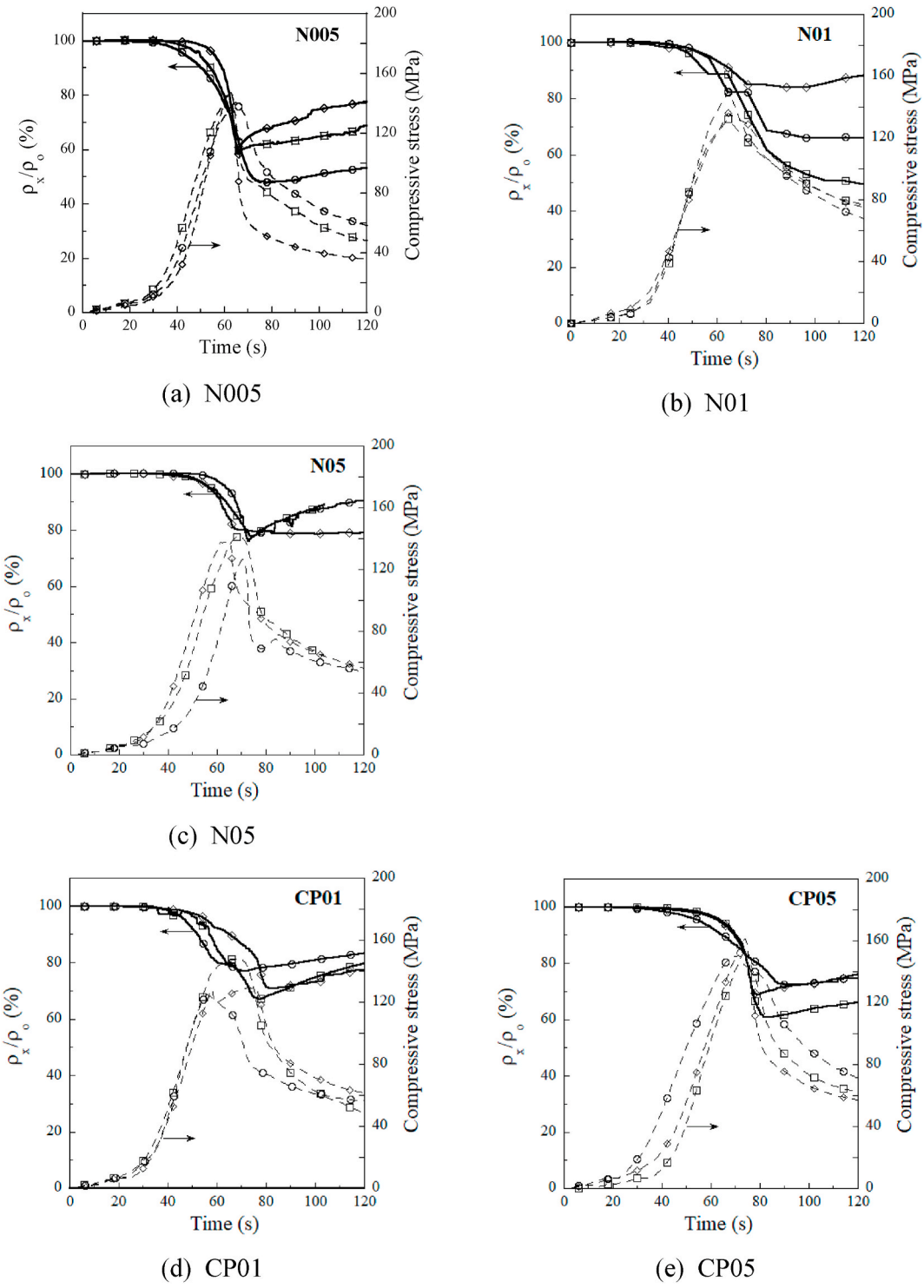

Fig. 8. Piezoresistive response of S–UHPCs containing different functional fillers under compression.

strength and density of the S–UHPCs. The compressive strength of the S–UHPCs containing NAs, CPAs, FSSAs, and MWCNTs was higher than that of S–UHPCs without additional functional fillers (154 MPa) [42]: the compressive strength of N005, N01, N05, CP01, CP05, S01, S01C01, and S05C01 was obtained as 156.1, 167.8, 156.0, 158.2, 165.0, 155.9, 159.1, and 160.1 MPa, respectively. The density of the S–UHPCs containing NAs or CPAs (N05 and CP05) was 2747 and 2712 kg/m^3, respectively, even higher than that (2573 kg/m^3) of the S–UHPCs containing FSSAs and MWCNTs (S05C01) and (2520 kg/m^3) of the S–UHPCs with no functional fillers owing to the higher density of NAs and CPAs as provided in Table 1.

The addition of functional fillers did not produce negative effects on the workability of S–UHPCs: the flow values of S-UHPC matrices were varied from 200 to 275 mm, as summarized in Table 2. However, the addition of MWCNTs decreased the workability of the S–UHPCs even though more amount of super-plasticizer was added. As provided in Table 2, the amount of super-plasticizer of S01 and S01C01 was 0.071 and 0.096, respectively, while the flow of those added suitable amount

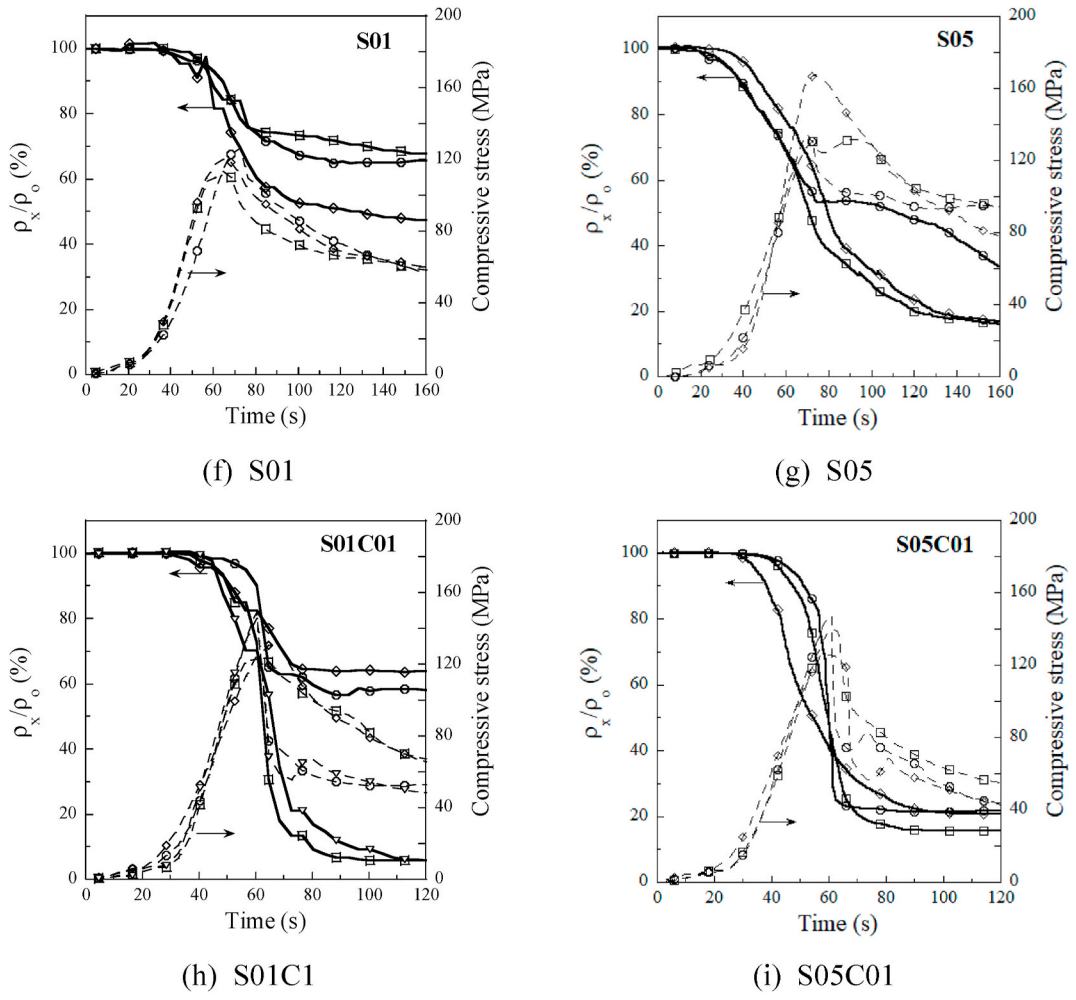

Fig. 8. (*continued*).

Table 3
Self-stress sensing characteristics of the S–UHPCs corresponding to the different functional fillers under compression.

Test series	ρ_o (kΩ-cm)	$\Delta\rho$ (kΩ-cm)	*FCR* (%)	σ_p, (MPa)	$SSC = FCR/\sigma_p$ (%/MPa)	Ref.
N005	975.4 (78.4)	268.4 (15.1)	27.5 (4.1)	144.8 (3.9)	0.190	
N01	817.0 (182.6)	165.5 (32.5)	20.6 (3.7)	140.1 (7.5)	0.147	
N05	284.6 (41.9)	44.6 (8.5)	15.6 (0.7)	135.4 (6.5)	0.115	
CP01	625.5 (49.7)	106.6 (14.3)	17.1 (2.6)	134.1 (9.9)	0.128	
CP05	140.8 (20.7)	22.1 (2.9)	15.8 (1.3)	155.2 (4.4)	0.102	
S01	1631.4 (25.7)	416.5 (82.1)	26.5 (8.4)	130.2 (10.8)	0.203	
S05	205.1 (3)	87.99 (6.8)	42.9 (4.0)	144 (16.5)	0.298	[44]
S01C01	765.7 (241.8)	248.3 (56.7)	33.62 (6.5)	139.3 (11.4)	0.241	
S05C01	189.1 (9.4)	107.3 (3.6)	56.8 (1.4)	138.6 (8.1)	0.410	

of super-plasticizer was obtained as 230 and 200 mm, respectively.

Fig. 10 shows the microstructure of the S–UHPCs while Fig. 11 does the uniform distribution of particle type functional fillers (NAs, CPAs, and FSSAs) and nano type functional fillers (MWCNTs) in the S–UHPCs. The interfacial transition zone surrounding functional fillers generally contained little porosity (Fig. 10) while the functional fillers were uniformly distributed in the S-UHPC matrices (Fig. 11).

5. Discussion

The conductive network of S–UHPCs, which was strongly dependent on both tunneling and contact conductions between the functional fillers [2,42,44]. Tunneling conduction is influenced by the distance between the functional fillers while contact conduction between functional fillers is dependent on the number of fibers and contacting fibers [2,42,44,52,53]. The addition of steel fibers generally enhanced contacting conduction whereas that of particle type functional fillers (NAs, CPAs, and FSSAs) and nano type functional fillers (MWCNTs) mainly did tunneling conduction. The electrical tunneling resistance (R_t) of a tunnel resistor between adjacent conductive functional fillers (carbon black) could be calculated by using Eq. (4) [52].

$$R_t = k_1 \cdot L \cdot \exp(k_2 \cdot L) \tag{4}$$

where $k_1 = (2/3)\cdot(2m\lambda)^{-1/2}\cdot(e/h)^{-2}\cdot A^{-1}$ and $k_2 = (4\pi/h)\cdot(2m\lambda)^{1/2}$ $k_2 = (4\pi/h).(2m\lambda)^{1/2}$ in which e is charge on an electron ($e = -1.602176634 \times 10^{-19}$ C), m is electron mass ($m = 9.10938356 \times 10^{-31}$ kg), λ is height of tunnel potential barrier, depending on the matrix property [52], and h is Planck's constant ($h = 6.62607015 \times 10^{-34}$ J s). The electrical contacting resistance (R_C) of composites with conductive fibers (such as carbon fibers) can be calculated by using Eq. (5) [53],

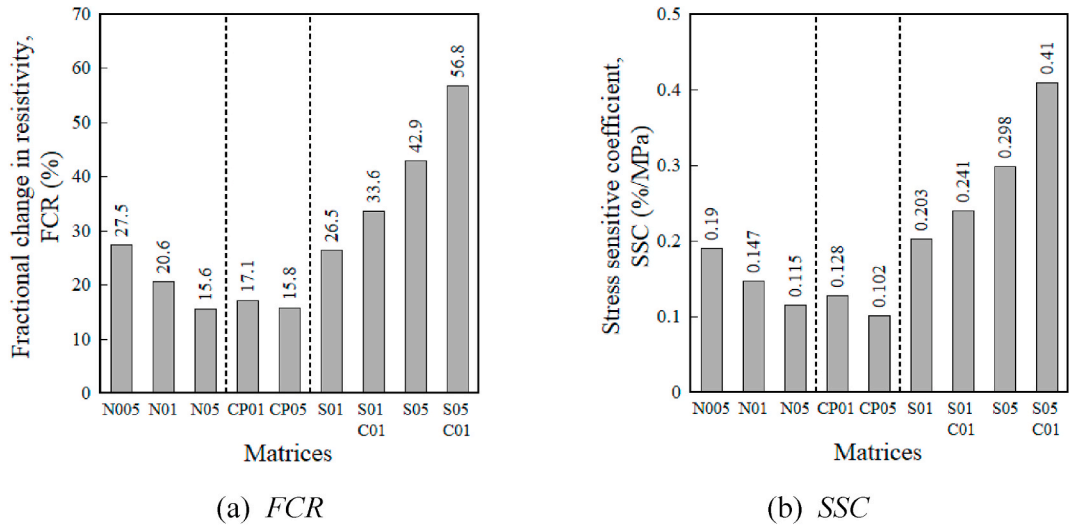

Fig. 9. Effect of functional filler content on *FCR* and *SSC* of S-UHPC.

Table 4
N_p, L, N_f, and N_c of the S–UHPCs.

Test series	Functional fillers	N_p	L (μm)	N_f	N_c
N005	NAs	1608149983	32.7	13262	10465
N01	NAs	3268682703	23.7	13262	10465
N05	NAs	17943543471	9.1	13262	10465
CP01	CPAs	1408046	334.6	13262	10465
CP05	CPAs	7030930	129.5	13262	10465
S01	FSSAs	103378	675.4	13262	10465
S05	FSSAs	656135	185.4	13262	10465
S10	FSSAs	1314006	66.5	13262	10465
S01C01	FSSAs	103378	675.4	13262	10465
S05C01	FSSAs	550396	220.1	13262	10465

$$R_C = \frac{N_A}{N_C} \cdot \frac{4\rho \cdot l}{\pi \cdot d_f^2} \cdot \frac{a}{\left(13.8 d_f \sqrt{1/V_o}\right)} \tag{5}$$

where V_o is the fiber volume fraction, N_C is the number of contacting fibers, N_A is the number of fibers per conductive path, a is the length of specimen, and l, d_f, and ρ are the length, diameter, and the electrical resistivity of conductive fibers, respectively.

Assuming that the particle type functional fillers were uniformly distributed in the matrix, the distance L, as can be seen in Fig. 12, between adjacent particle type functional fillers and the number of particle type functional fillers (N_p) could be calculated by using Eqs. (6) and (7), respectively, as provided in Table 4 [35]. Further, the number of fibers (N_f) and contacting fibers (N_c) could be calculated using Eqs. (8) and (9), respectively, as provided in Table 4 [36].

$$L = d_p \cdot \left(\left(\frac{\pi}{6}\right)^{1/3} \cdot V_p^{(-1/3)} - 1 \right) \tag{6}$$

$$N_p = \frac{V_p \cdot V_C}{V_{pp}} = \frac{V_p \cdot V_C}{\frac{4}{3}\pi \cdot \left(\frac{d_p}{2}\right)^3} \tag{7}$$

$$N_f = \frac{V_o \cdot V_C}{V_F} = \frac{V_o \cdot V_C}{\pi {d_f}^2 \cdot \sqrt{\frac{1}{V_o}}} \tag{8}$$

$$N_C = \frac{8 V_o \cdot V_C \cos^{-1}\left(\frac{13.8 d_f}{l}\sqrt{\frac{1}{V_o}}\right)}{\left(\pi d_f\right)^2 l} \tag{9}$$

where V_p is the volume content of particle type functional fillers, V_C is the volume of composite, V_{pp} is the volume of a single particle type functional fillers, V_o is the fiber volume fraction, V_F is the volume of a fiber, d_p is the diameter of a single particle type functional fillers, and d_f is the diameter of a fiber.

5.1. Effects of particle type functional fillers (NAs, CPAs, and FSSAs)

The electrical conductivity of the FFs had considerable effects on the electrical resistivity of the S–UHPCs than the distance between the FFs. The distance between the CPAs in CP05 was calculated as 129.5 μm, further than the distance (9.1 μm) between the smaller NAs in N05 but closer than that (220.1 μm) of the larger FSSAs in S05. Despite the further distance (129.5 μm) between the CPAs in CP05, CP05 produced the lowest electrical resistance, as shown in Fig. 9. The higher electrical conductivity of the S–UHPCs containing CPAs was attributed to the higher electrical conductivity of CPAs, as provided in Table 1.

FSSAs were found to be suitable functional fillers for S–UHPCs and much lower cost than the CPAs and NAs (Table 1). The S–UHPCs containing FSSAs generally produced higher *FCRs* and Δρ than the S–UHPCs containing other particle type functional fillers including CPAs and NAs, regardless of the contents of particle type functional fillers. The lower *FCR* of the S–UHPCs containing CPAs and NAs would be attributed to the highly conductive pathways initially formed in the microstructure. While the lower initial electrical resistivity of them would be due to the shorter distance between functional fillers (Table 4) and higher material electrical conductivity (Table 1). Fig. 13 shows the effect of initial distance L between particle type functional fillers on the *FCR*: the *FCR* of S–UHPCs with a higher content of NAs or CPAs (N05 or CP05, respectively) was lower than that of N005 or CP01, respectively. However, the *FCR* of the S-UHPC containing FSSAs increased as the functional fillers to cement ratio increased from 0.1 (S01) to 0.5 (S05) but it decreased as the functional fillers to cement ratio further increased from 0.5 (S05) to 1.0 (S10). Wang et al. [37] also reported that the self-sensing capacity of smart concrete containing carbon fibers under an applied load initially increased and then decreased as the content of carbon fibers increased. The reduction of *FCR* at higher content of functional fillers, i.e., shorter distance L between functional fillers, was originated from the lower initial electrical resistance of S–UHPCs containing functional fillers more than percolation threshold content of functional fillers [2,35,36]. S05, containing functional fillers below the percolation threshold, could generate higher *FCR* when it was under compression because the change in the electrical resistance could increase while the initial electrical resistivity was relatively low. Under compression, the conductive partially

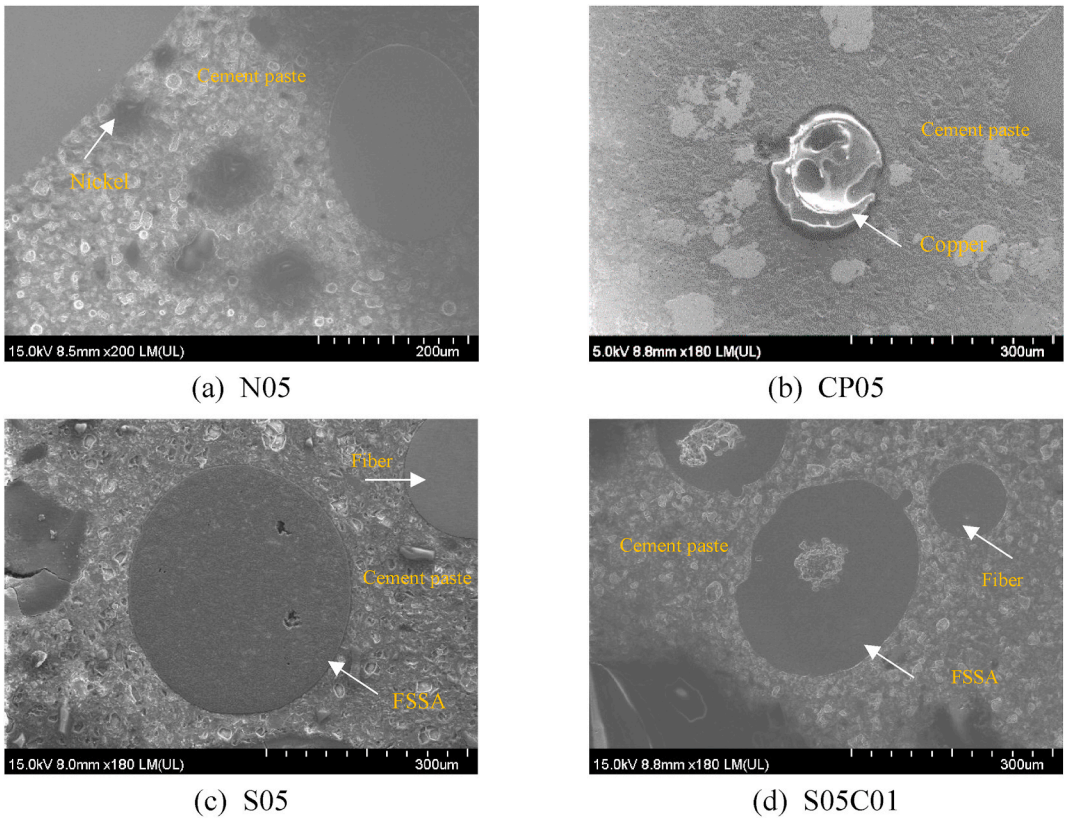

Fig. 10. FE-SEM images of the S-UHPC microstructures.

continuous paths in S05 could be converted into conductive continuous paths owing to the tunneling effect and the formation of direct connections.

These findings clearly demonstrated that both the content and electrical conductivity of the functional fillers were important factors in building the conductive networks in the S-UHPC and changing the piezoresistive response of the S–UHPCs. S05 had a suitable content and good electrical conductivity of the FSSAs, thereby producing a conductive network and a higher *FCR* (and self-stress sensing capacity) under compression.

5.2. Effects of nano type functional fillers (MWCNTs)

The addition of MWCNTs clearly improved the FCRs of S–UHPCs, as shown in Fig. 9. S05C01 containing 2 vol% steel fibers, FSSAs with functional fillers to cement ratio of 0.5, and MWCNTs with functional filler to cement ratio of 0.1% produced the highest fractional change in electrical resistivity (56.8%) and stress sensitivity coefficient (0.41%/MPa) in comparison with other investigated S–UHPCs.

Fig. 14 illustrates the conductive network response of S–UHPCs containing MWCNTs, FSSAs, and steel fibers. The addition of 2 vol% steel fibers and particle type functional filler (FSSAs with functional filler to cement ratio of 0.5) enhanced the conductive network of the S–UHPCs at the micro level, as investigated in previous parts. Besides, the nano type functional fillers (MWCNTs with functional filler to cement ratio of 0.1%) enhanced the conductive network of the S–UHPCs at nano level under compression (Fig. 14b). A large number of MWCNTs (53903869365908) calculated using Eq. (7), uniformly distributed in the S–UHPCs (Fig. 11d) decreased the distance between the functional fillers, increased the number of contact between functional fillers, and consequently increased both tunneling and contacting conduction of the functional fillers within S–UHPCs under compression.

The content and type of functional fillers should be carefully determined to achieve higher self-sensing capacity in S–UHPCs. Lee et al. [42] reported that the S–UHPCs containing 2 vol% steel fibers and MWCNTs with functional filler to cement of 0.5% produced a lower *FCR* than that containing only 2 vol% steel fibers because the content of functional fillers including MWCNTs and fibers would exceed the percolation threshold. S05C01 generated the best electrically conductive network structure with a combination of fiber, particle (FSSAs), and nano type functional fillers and consequently produced the highest *FCR* under compression.

6. Conclusions

The self-stress sensing ability of S–UHPCs was enhanced by adding different functional fillers, including particle type functional fillers (CPAs, NAs, and FSSAs), fiber type functional fillers (steel fibers), and nano type functional fillers (MWCNTs). The particle type functional fillers were used to partially replace silica sands in the matrix to facilitate uniform distribution of the functional fillers in the UHPC matrices. The fiber type functional fillers were added to all matrices for enhanced electrical conductive networks and crack-resistance. The nano type functional fillers were added to improve the conductive network and piezoresistive response of the S–UHPCs under compression. The following conclusions were drawn:

- The addition of particle type functional fillers (NAs, CPAs, and FSSAs) clearly enhanced the electrical conductivity of the S–UHPCs.
- Both the content and electrical conductivity of the functional fillers were important factors in building the conductive networks in the S-UHPC and changing the piezoresistive response of the S–UHPCs.
- The initial electrical resistivity of S–UHPCs containing CPAs with 0.5% (CP05) was lowest (140.8 kΩ-cm), thus the initial electrical conductivity of those was higher than that of S–UHPCs containing NAs and FSSAs.

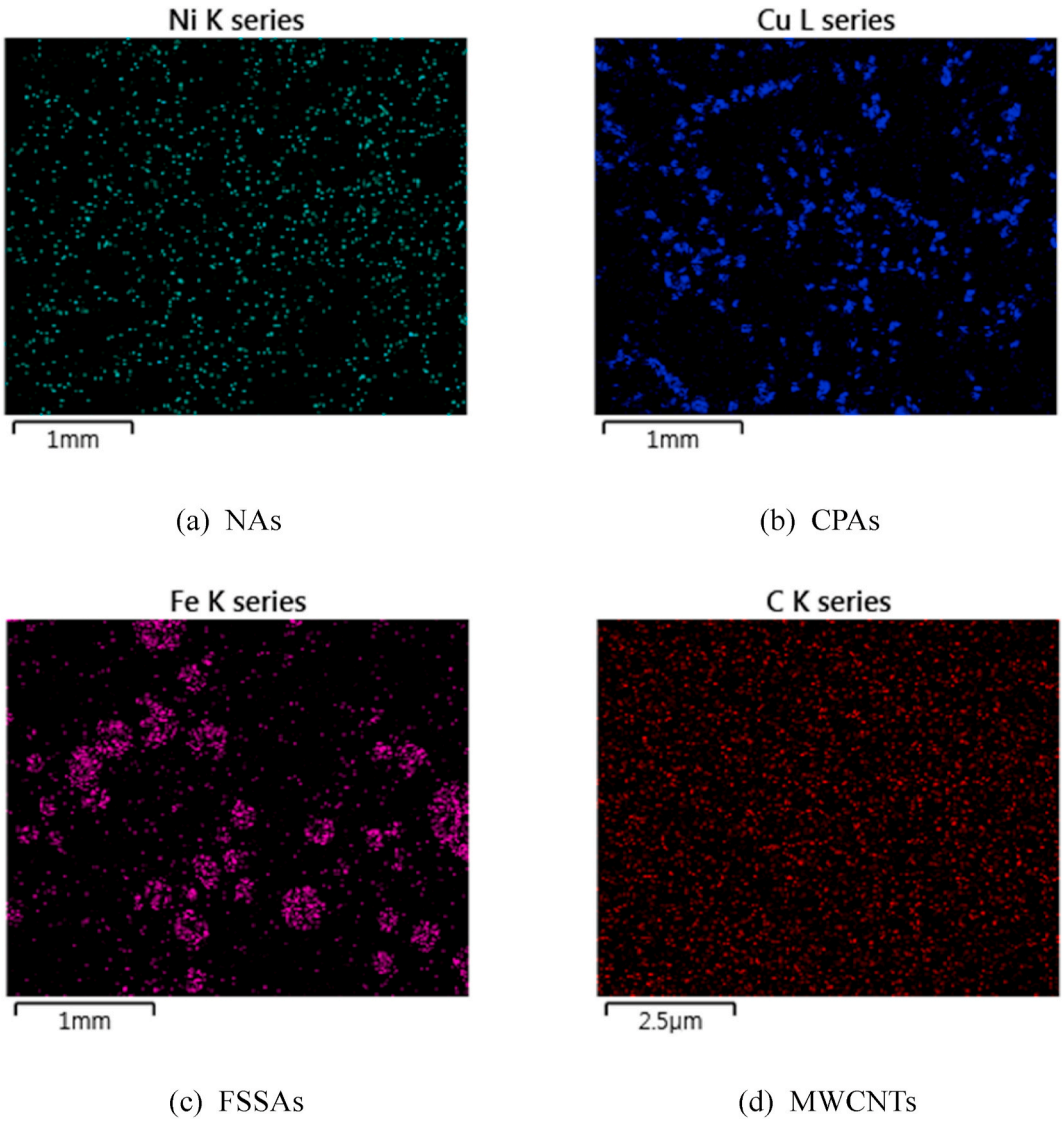

Fig. 11. EDS images of the functional filler distribution in the S–UHPCs.

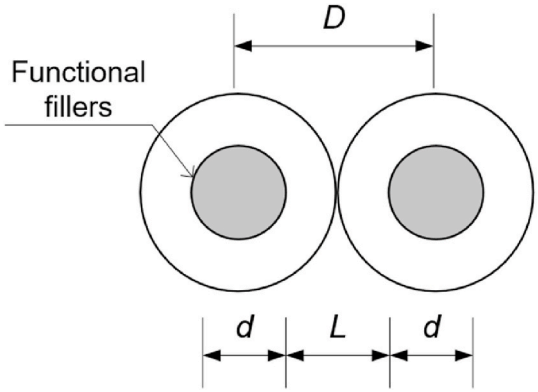

Fig. 12. Distance between particle type functional fillers.

- FSSAs were found to be suitable functional fillers for S–UHPCs and much lower cost than the CPAs and NAs. S05 with a suitable content and electrical conductivity of functional fillers generated a good conductive network and consequently produced higher *FCR (42.9%)* and higher *SSC* (0.298%/MPa) under compression than S–UHPCs containing CPAs and NAs. The lower FCR of the S–UHPCs containing CPAs and NAs would be attributed to the highly conductive pathways initially formed in the microstructure owing to higher percolation threshold content of functional fillers.
- The addition of nano type functional fillers enhanced the conductive network of S–UHPCs at the nano level and consequently notably increased the electrical conductivity, *FCR*, and *SSC* of the S–UHPCs. S05C01 exhibited the highest *FCR* (56.8%) and stress sensitivity coefficient (0.41%/MPa) among all the S-UHPC samples.

The findings of this study demonstrated that a conductive network of S–UHPCs can be achieved using a combination of different types of functional fillers, namely fiber and particle types, with varying sizes, namely micro- and nano-level, where a suitable composition can maximize the self-stress sensing properties of S–UHPCs under compression.

Author statement

Huy Viet LE: Investigation, Methodology, Writing- Original draft preparation.
Min Kyoung KIM: Writing- Reviewing and Editing.
Seon Uk KIM: Investigation.
Sang-Yeop CHUNG: Writing- Reviewing and Editing.

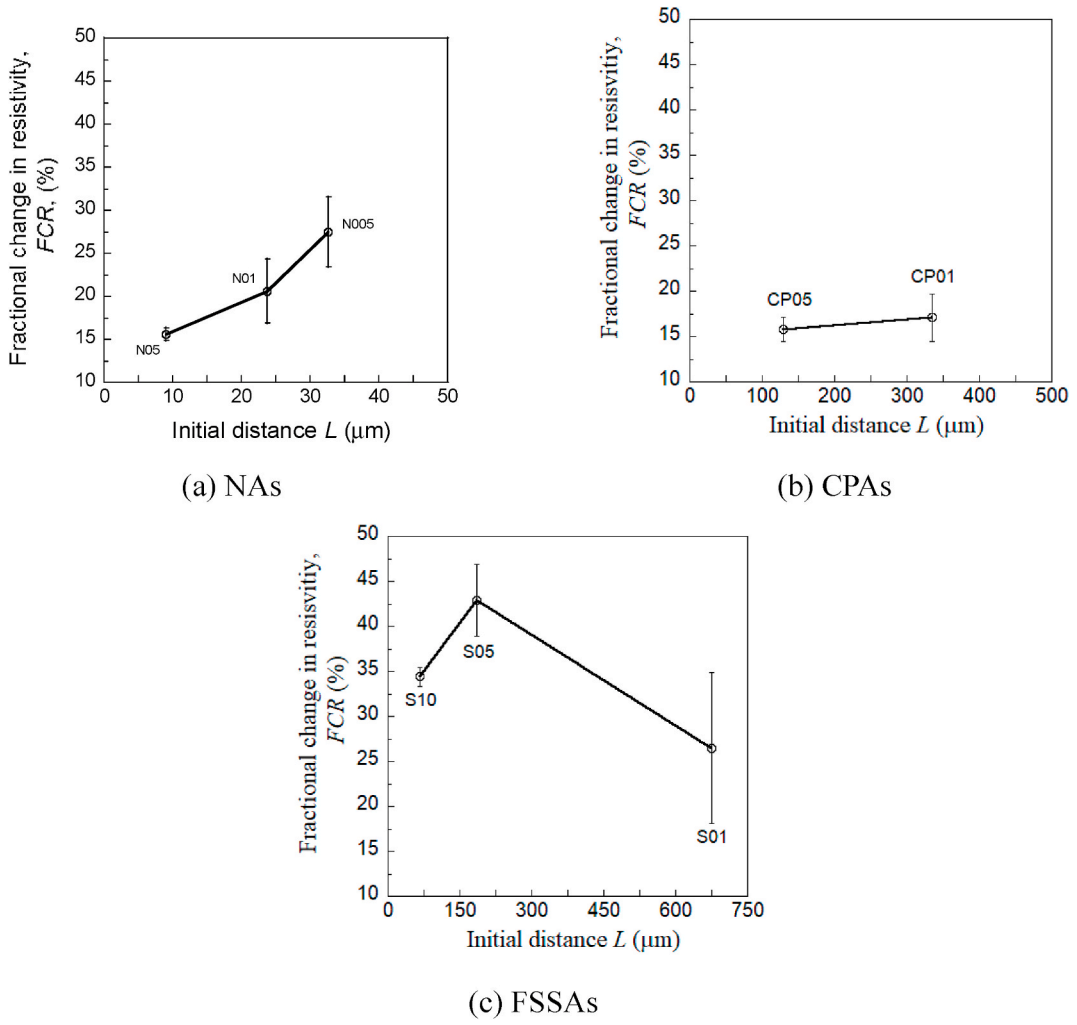

Fig. 13. Correlation between *FCR* and initial distance of functional fillers.

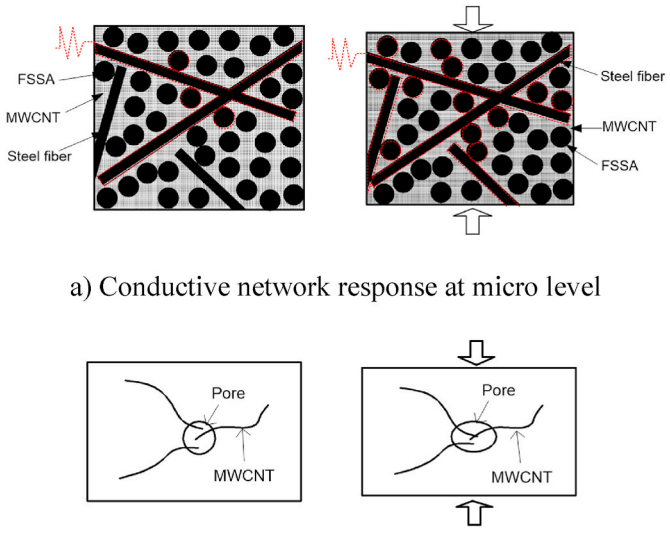

Fig. 14. Conductive network model of S–UHPCs containing a mixture of different functional fillers under compression.

Dong Joo KIM: Methodology, Writing- Reviewing and Editing, Supervision.

Declaration of competing interest

The authors declare that they have no known competing financial interests or personal relationships that could have appeared to influence the work reported in this paper.

Acknowledgments

This work is supported by the Korea Agency for Infrastructure Technology Advancement (KAIA) grant funded by the Ministry of Land, Infrastructure and Transport (Grant 21NANO-B156177-02).

References

[1] D.J. Kim, H.W. Noh, S.I. Choi, R.H. Hwang, S.Y. Lee, Smart Concrete Anchorage for Monitoring Pre-stressing Loss, KoreaPatent. Submitted (2019).
[2] B. Han, X. Yu, J. Ou, Self-sensing Concrete in Smart Structures, Butterworth Heinemann, Elsevier, Kidlington, 2014, https://doi.org/10.1016/C2013-0-14456-X.
[3] A. Al-Dahawi, O. Öztürk, F. Emami, G. Yildirim, M. Şahmaran, Effect of mixing methods on the electrical properties of cementitious composites incorporating different carbon-based materials, Construct. Build. Mater. 104 (2016) 160–168, https://doi.org/10.1016/j.conbuildmat.2015.12.072.
[4] A. Al-Dahawi, G. Yıldırım, O. Öztürk, M. Şahmaran, Assessment of self-sensing capability of Engineered Cementitious Composites within the elastic and plastic

ranges of cyclic flexural loading, Construct. Build. Mater. 145 (2017) 1–10, https://doi.org/10.1016/j.conbuildmat.2017.03.236.
[5] A. Al-Dahawi, M.H. Sarwary, O. Öztürk, G. Yildirim, A. Akin, M. Şahmaran, M. Lachemi, Electrical percolation threshold of cementitious composites possessing self-sensing functionality incorporating different carbon-based materials, Smart Mater. Struct. 25 (2016), https://doi.org/10.1088/0964-1726/25/10/105005.
[6] G. Yıldırım, O. Öztürk, A. Al-Dahawi, A. Afşın Ulu, M. Şahmaran, Self-sensing capability of engineered cementitious composites: effects of aging and loading conditions, Construct. Build. Mater. 231 (2020), https://doi.org/10.1016/j.conbuildmat.2019.117132.
[7] M.H. Sarwary, G. Yildirim, A. Al-Dahawi, Ö. Anil, K.A. Khiavi, K. Toklu, M. Şahmaran, Self-sensing of flexural damage in large-scale steel-reinforced mortar beams, ACI Mater. J. 116 (2019) 209–221, https://doi.org/10.14359/51715581.
[8] F.I. Mussa, A.M. Al-Dahawi, Q.S. Banyhussan, M.R. Baanoon, M.A. Shalash, Carbon fiber-reinforced Asphalt concrete: an investigation of some electrical and mechanical properties, IOP Conf. Ser. Mater. Sci. Eng. 737 (2020), https://doi.org/10.1088/1757-899X/737/1/012122.
[9] A.M. Al-Dahawi, Effect of curing age on the self-sensing behavior of carbon-based engineered cementitious composites (ECC) under monotonic flexural loading scenario, MATEC Web Conf 162 (2018) 250–257, https://doi.org/10.1051/matecconf/201816201034.
[10] G. Yıldırım, M.H. Sarwary, A. Al-Dahawi, O. Öztürk, Ö. Anıl, M.S. ahmaran, Piezoresistive behavior of CF- and CNT-based reinforced concrete beams subjected to static flexural loading: shear failure investigation, Construct. Build. Mater. 168 (2018) 266–279, https://doi.org/10.1016/j.conbuildmat.2018.02.124.
[11] E. Demircilioğlu, E. Teomete, E. Schlangen, F.J. Baeza, Temperature and moisture effects on electrical resistance and strain sensitivity of smart concrete, Construct. Build. Mater. 224 (2019) 420–427, https://doi.org/10.1016/j.conbuildmat.2019.07.091.
[12] S. Wen, D.D.L. Chung, A comparative study of steel- and carbon-fiber cement as piezoresistive strain sensors, Adv. Cement Res. 15 (2003) 119–128.
[13] D.D.L. Chung, Piezoresistive cement-based materials for strain sensing, J. Intell. Mater. Syst. Struct. 13 (2002) 599–609, https://doi.org/10.1106/104538902031861.
[14] Z.Q. Shi, D.D.L. Chung, Carbon fiber-reinforced concrete for traffic monitoring and weighing in motion, Cement Concr. Res. 29 (1999) 435–439, https://doi.org/10.1016/S0008-8846(98)00204-X.
[15] X. Fu, W. Lu, D.D.L. Chung, Improving the strain-sensing ability of carbon fiber-reinforced cement by ozone treatment of the fibers, Cement Concr. Res. 28 (1998) 183–187, https://doi.org/10.1016/S0008-8846(97)00265-2.
[16] D.M. Bontea, D.D.L. Chung, G.C. Lee, Damage in carbon fiber-reinforced concrete, monitored by electrical resistance measurement, Cement Concr. Res. 30 (2000) 651–659, https://doi.org/10.1016/S0008-8846(00)00204-0.
[17] B. Han, J. Ou, Embedded piezoresistive cement-based stress/strain sensor, Sensors Actuators, A Phys. 138 (2007) 294–298, https://doi.org/10.1016/j.sna.2007.05.011.
[18] D.D.L. Chung, Self-monitoring structural materials, Mater. Sci. Eng. R Rep. 22 (1998) 57–78, https://doi.org/10.1016/S0927-796X(97)00021-1.
[19] J. Donnini, T. Bellezze, V. Corinaldesi, Mechanical, electrical and self-sensing properties of cementitious mortars containing short carbon fibers, J. Build. Eng. 20 (2018) 8–14, https://doi.org/10.1016/j.jobe.2018.06.011.
[20] Y. Wang, Y. Wang, B. Han, B. Wan, G. Cai, Z. Li, Strain monitoring of concrete components using embedded carbon nanofibers/epoxy sensors, Construct. Build. Mater. 186 (2018) 367–378, https://doi.org/10.1016/j.conbuildmat.2018.07.147.
[21] A.O. Monteiro, P.B. Cachim, P.M.F.J. Costa, Electrical properties of cement-based composites containing carbon black particles, Mater. Today Proc. 2 (2015) 193–199, https://doi.org/10.1016/j.matpr.2015.04.021.
[22] Y. Ding, G. Liu, A. Hussain, F. Pacheco-torgal, Y. Zhang, Effect of steel fiber and carbon black on the self-sensing ability of concrete cracks under bending, Construct. Build. Mater. 207 (2019) 630–639, https://doi.org/10.1016/j.conbuildmat.2019.02.160.
[23] G.H. Nalon, J.C.L. Ribeiro, E.N.D. de Araújo, L.G. Pedroti, J.M.F. de Carvalho, R. F. Santos, A. Aparecido-Ferreira, Effects of different kinds of carbon black nanoparticles on the piezoresistive and mechanical properties of cement-based composites, J. Build. Eng. 32 (2020), https://doi.org/10.1016/j.jobe.2020.101724.
[24] E. García-Macías, A. Downey, A. D'Alessandro, R. Castro-Triguero, S. Laflamme, F. Ubertini, Enhanced lumped circuit model for smart nanocomposite cement-based sensors under dynamic compressive loading conditions, Sensors Actuators, A Phys. 260 (2017) 45–57, https://doi.org/10.1016/j.sna.2017.04.004.
[25] D.Y. Yoo, S. Kim, S.H. Lee, Self-sensing capability of ultra-high-performance concrete containing steel fibers and carbon nanotubes under tension, Sensors Actuators, A Phys. 276 (2018) 125–136, https://doi.org/10.1016/j.sna.2018.04.009.
[26] B. Han, X. Yu, E. Kwon, A self-sensing carbon nanotube/cement composite for traffic monitoring, Nanotechnology 20 (2009) 1–5, https://doi.org/10.1088/0957-4484/20/44/445501.
[27] D.Y. Yoo, I. You, S.J. Lee, Electrical properties of cement-based composites with carbon nanotubes, graphene, and graphite nanofibers, Sensors 17 (2017) 1–13, https://doi.org/10.3390/s17051064.
[28] M.S. Konsta-gdoutos, A.A. Chrysoula, Self sensing carbon nanotube (CNT) and nanofiber (CNF) cementitious composites for real time damage assessment in smart structures, Cement Concr. Compos. 53 (2014) 162–169, https://doi.org/10.1016/j.cemconcomp.2014.07.003.
[29] B. Han, X. Yu, E. Kwon, J. Ou, Sensing properties of CNT-filled cement-based stress sensors, J. Civ. Struct Heal. Monit. 1 (2011) 17–24, https://doi.org/10.1007/s13349-010-0001-5.
[30] S. Ding, Y. Ruan, X. Yu, B. Han, Y. Ni, Self-monitoring of smart concrete column incorporating CNT/NCB composite fillers modified cementitious sensors, Construct. Build. Mater. 201 (2019) 127–137, https://doi.org/10.1016/j.conbuildmat.2018.12.203.
[31] J. Luo, C. Zhang, Z. Duan, B. Wang, Q. Li, K.L. Chung, J. Zhang, S. Chen, Influences of multi-walled carbon nanotube (MCNT) fraction, moisture, stress/strain level on the electrical properties of MCNT cement-based composites, Sensors Actuators, A Phys. 280 (2018) 413–421, https://doi.org/10.1016/j.sna.2018.08.010.
[32] B. Han, K. Zhang, X. Yu, E. Kwon, J. Ou, Electrical characteristics and pressure-sensitive response measurements of carboxyl MWNT/cement composites, Cement Concr. Compos. 34 (2012) 794–800, https://doi.org/10.1016/j.cemconcomp.2012.02.012.
[33] A. Downey, A. D'Alessandro, F. Ubertini, S. Laflamm, R. Geiger, Biphasic DC measurement approach for enhanced measurement stability and multi- channel sampling of self-sensing multi- functional structural materials doped with carbon-based additives, Smart Mater. Struct. 26 (2017), 065008.
[34] A. Downey, A. D'Alessandro, M. Baquera, E. García-Macías, D. Rolfes, F. Ubertini, S. Laflamme, R. Castro-Triguero, Damage detection, localization and quantification in conductive smart concrete structures using a resistor mesh model, Eng. Struct. 148 (2017) 924–935, https://doi.org/10.1016/j.engstruct.2017.07.022.
[35] E. García-Macías, L. Rodríguez-Tembleque, A. Sáez, F. Ubertini, Crack detection and localization in RC beams through smart MWCNT/epoxy strip like strain sensors, Smart Mater. Struct. 27 (2018) 115022.
[36] S. Sun, B. Han, S. Jiang, X. Yu, Y. Wang, H. Li, J. Ou, Nano graphite platelets-enabled piezoresistive cementitious composites for structural health monitoring, Construct. Build. Mater. 136 (2017) 314–328, https://doi.org/10.1016/j.conbuildmat.2017.01.006.
[37] B. Han, K. Zhang, X. Yu, E. Kwon, J. Ou, Nickel particle-based self-sensing pavement for vehicle detection, Meas. J. Int. Meas. Confed. 44 (2011) 1645–1650, https://doi.org/10.1016/j.measurement.2011.06.014.
[38] S. Wen, D.D.L. Chung, A comparative study of steel- and carbon-fibre cement as piezoresistive strain sensors, Adv. Cement Res. 15 (2003) 119–128, https://doi.org/10.1680/adcr.15.3.119.36621.
[39] H.V. Le, D.J. Kim, Effects of matrix strength, fiber type, and fiber content on the electrical resistivity of steel-fiber-reinforced cement composites during fiber pullout, J. Korean Soc. Civ. Eng. 39 (2019) 675–689.
[40] H.V. Le, D.J. Kim, Detecting crack and damage location in self-sensing fiber reinforced cementitious composites, Construct. Build. Mater. 240 (2020) 117973, https://doi.org/10.1016/j.conbuildmat.2019.117973.
[41] H.V. Le, D.J. Kim, Effect of matrix cracking on electrical resistivity of high performance fiber reinforced cementitious composites in tension, Construct. Build. Mater. 156 (2017) 750–760, https://doi.org/10.1016/j.conbuildmat.2017.09.046.
[42] S.Y. Lee, H.V. Le, D.J. Kim, Self-stress sensing smart concrete containing fine steel slag aggregates and steel fibers under high compressive stress, Construct. Build. Mater. 220 (2019) 149–160, https://doi.org/10.1016/j.conbuildmat.2019.05.197.
[43] I. You, D.Y. Yoo, S. Kim, M.J. Kim, G. Zi, Electrical and self-sensing properties of ultra-high-performance fiber-reinforced concrete with carbon nanotubes, Sensors 17 (2017) 1–19, https://doi.org/10.3390/s17112481.
[44] H.V. Le, D.H. Lee, D.J. Kim, Effects of steel slag aggregate size and content on piezoresistive responses of smart ultra-high-performance fiber-reinforced concretes, Sensors Actuators, A Phys. 305 (2020) 111925, https://doi.org/10.1016/j.sna.2020.111925.
[45] X. Hu, C. Shi, X. Liu, J. Zhang, G. de Schutter, A review on microstructural characterization of cement-based materials by AC impedance spectroscopy, Cement Concr. Compos. 100 (2019) 1–14, https://doi.org/10.1016/j.cemconcomp.2019.03.018.
[46] R.B. Polder, Test methods for on site measurement of resistivity of concrete - a RILEM TC-154 technical recommendation, Construct. Build. Mater. 15 (2001) 125–131, https://doi.org/10.1016/S0950-0618(00)00061-1.
[47] W.J. McCarter, R. Brousseau, The A.C. response of hardened cement paste, Cement Concr. Res. 20 (1990) 891–900.
[48] J.M. Torrents, T.O. Mason, E.J. Garboczi, Impedance spectra of fiber-reinforced cement-based composites: a modeling approach, Cement Concr. Res. 30 (2000) 585–592, https://doi.org/10.1016/S0008-8846(00)00211-8.
[49] C.G. Berrocal, K. Hornbostel, M.R. Geiker, L. Ingemar, K. Lundgren, D.G. Bekas, Electrical resistivity measurements in steel fibre reinforced cementitious materials, Cement Concr. Compos. 89 (2018) 216–229, https://doi.org/10.1016/j.cemconcomp.2018.03.015.
[50] A. Peled, J.M. Torrents, T.O. Mason, S.P. Shah, E.J. Garboczi, Electrical impedance spectra to monitor damage during tensile loading of cement composites, ACI Mater. J. 98 (2001) 313–322, https://doi.org/10.14359/10400.
[51] H.V. Le, M.K. Kim, D.J. Kim, J. Park, Electrical properties of smart ultra-high performance concrete under various temperatures, humidities, and age of concrete, Cement Concr. Compos. 118 (2021) 103979, https://doi.org/10.1016/j.cemconcomp.2021.103979.
[52] H. Xiao, H. Li, J. Ou, Modeling of piezoresistivity of carbon black filled cement-based composites under multi-axial strain, Sensor Actuator Phys. 160 (2010) 87–93, https://doi.org/10.1016/j.sna.2010.04.027.
[53] J. Xu, W. Zhong, W. Yao, Modeling of conductivity in carbon fiber-reinforced cement-based composite, J. Mater. Sci. (2010) 3538–3546, https://doi.org/10.1007/s10853-010-4396-5.

[54] B. Han, S. Ding, X. Yu, Intrinsic self-sensing concrete and structures: a review, Measurement 59 (2015) 110–128, https://doi.org/10.1016/j.measurement.2014.09.048.
[55] F.C. Walsh, Electrode reactions in metal finishing, Trans. Inst. Met. Finish. 69 (1991) 107–110, https://doi.org/10.1080/00202967.1991.11870904.
[56] Hitachi, Ultra-high resolution scaning electron microscope SU8000 Series. https://hitachi-hta.com/sites/default/files/literature/SU8000FamilyBrochure.pdf.
[57] J.J. Kim, D.J. Kim, S.T. Kang, J.H. Lee, Influence of sand to coarse aggregate ratio on the interfacial bond strength of steel fibers in concrete for nuclear power plant, Nucl. Eng. Des. 252 (2012) 1–10, https://doi.org/10.1016/j.nucengdes.2012.07.004.